Experiment to search for P- and T-violating interactions in the hyperfine structure of thallium fluoride

Edward A. Hinds* and P. G. H. Sandars
Clarendon Laboratory, Oxford University, Oxford, England
(Received 29 March 1979)

The authors describe a molecular-beam-resonance experiment to search for P- and T-violating interactions in the thallium fluoride molecule. Specifically the interactions looked for are of the form $\mathcal{H}_{PT} = d\hat{\sigma}_{Tl}\cdot\hat{\lambda}_{TlF}$, where d is a coupling constant, $\hat{\sigma}_{Tl}$ is a unit vector parallel to the spin angular momentum of the thallium nucleus, and $\hat{\lambda}_{TlF}$ is a unit vector along the internuclear axis. The null result of the experiment is $d/h = 11\pm42$ mHz. This result implies new upper limits on the electric dipole moment of the proton and on a possible weak, P- and T-violating, neutral-current tensor interaction.

I. INTRODUCTION

A molecular-beam-resonance experiment has been carried out to search for simultaneous violation of parity P and time reversal invariance T in a molecule. The null result has been used to place upper limits on both the electric dipole moment (edm) of the proton and a possible, P and T violating, weak neutral current interaction between electrons and nucleons.[1]

The existence of a permanent edm on an elementary particle is forbidden if either P or T is an exact symmetry. Interest in T violation stems largely from the discovery of a CP violating decay ($K_L^0 \to 2\pi$) of the long lived kaon,[2] which implies, through the CPT theorem, that T is violated in the K^0 system. There is also direct evidence[3] that this is the case. As yet no experimental evidence has been found for T violation outside the K^0 system.

Ramsey *et al.*[4] have carried out a series of sensitive experiments to look for a neutron edm using beam-resonance techniques. An independent measurement of the proton edm is clearly worthwhile, but it is difficult to obtain comparable sensitivity because the proton is charged and therefore an experiment such as Ramsey's is impossible on free protons. Experiments in which the proton is bound in a neutral system would also appear unprofitable at first sight because of a general theorem[5] to the effect that the energy of a charged, point particle, in equilibrium under electrostatic forces has no contribution to its energy linear in its edm. Fortunately this theorem does not apply exactly to an atomic nucleus because it has finite size and structure, and we show in the preceding paper that in thallium fluoride (TlF) there is a first-order effect of sufficient size to provide a useful measurement of the proton edm. The choice of TlF as a suitable system to look for P and T violating interactions has been discussed elsewhere.[6]

An additional feature of atomic systems is that one can look for hyperfine structure arising from the weak interaction. Recent advances in the study of weak interactions have stimulated considerable interest in the detailed structure of the weak neutral current and at present it seems possible that there are parity-violating effects of order G in atoms.[7-14] We have shown[1] that if there is also T violation in such an interaction, there can be a first-order energy shift in TlF qualitatively similar to that produced by a nuclear electric dipole interaction.

A molecular beam has been used to observe a resonance of the ^{205}Tl nucleus in TlF in the presence of parallel electric and magnetic fields. Any shift of the resonant frequency which depends on the relative directions of the two fields $\vec{E}$ and $\vec{B}$ indicates the existence of a P and T violating interaction in the molecule. Specifically we are interested in detecting a P and T violating interaction of the form

$$\mathcal{H}_{PT} = d\hat{\sigma}_{Tl}\cdot\hat{\lambda}_{TlF}\,, \tag{1}$$

in which $\hat{\sigma}_{Tl}$ is a unit vector parallel to the spin of the Tl nucleus, and $\hat{\lambda}_{TlF}$ is a unit vector along the internuclear axis, directed towards the F nucleus. In the absence of an external electric field, there is no first-order energy contribution since $\hat{\lambda}_{TlF}$ is perpendicular to $\hat{\sigma}$. However, an external electric field parallel to the z axis will polarize the molecule and then $\hat{\sigma}_{Tl}\cdot\hat{\lambda}_{TlF}$ does not vanish. The level shifts due to $\mathcal{H}_{PT}$ in external electric and magnetic fields are shown in Fig. 1. The splittings W_p and W_a correspond to parallel and antiparallel external fields, respectively. The frequency shift P that we measure is given by

$$hP = (W_p - W_a) = 4d\langle\hat{\sigma}_{Tl}\cdot\hat{\lambda}_{TlF}\rangle. \tag{2}$$

The hyperfine structure of TlF is discussed in Sec. II as a preliminary to our detailed description of the experiment in Secs. III and IV. Results are given in Sec. V. Finally, in Sec. VI, we give in-

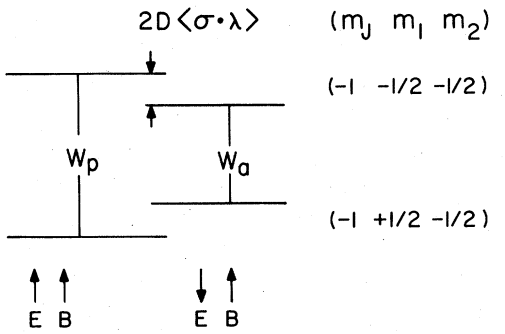

FIG. 1. Schematic diagram of the states involved in the main resonance. We show the level shifts when E is reversed, due to an interaction $d\hat{\sigma}_{\mathrm{Tl}}\cdot\hat{\lambda}_{\mathrm{TlF}}$ with positive d. m_J, m_1, and m_2 are the magnetic quantum numbers of molecular rotation, Tl nuclear spin, and F nuclear spin, respectively.

terpretations of our result in terms of a possible electric dipole moment d_p on the proton and a possible P and T violating weak neutral current.

II. GROUND-STATE STRUCTURE OF TlF

This experiment involves the $^1\Sigma$ electronic ground state and $v=0$ vibrational ground state of TlF. The largest structure of interest here is due to the rotational angular momentum J. In particular we are interested in the Stark effect of the $J=1$ rotational states. Figure 2 shows the expectation value of λ_z as a function of external electric field strength E_z, where λ_z is the z component of the unit vector $\hat{\lambda}$. These curves are derived from an expression for rigid rotators given by Lamb in an article by Hughes.[15] They are useful in evaluating $\hat{\sigma}\cdot\hat{\lambda}$ and in discussing the deflection of the beam in an inhomogeneous electric field.

In addition to the rotational structure there is hyperfine structure which arises from the coupling of rotational angular momentum (J,m_J) to the spin of the Tl nucleus (I_1,m_1) and the spin of the F nucleus (I_2,m_2). Throughout this work the subscripts 1 and 2 will refer to the Tl and F nuclei, respectively. In external electric and magnetic fields $\vec{\mathbf{E}}$ and $\vec{\mathbf{B}}$, the effective Hamiltonian for matrix elements diagonal in J involves the terms given in Table I. Values of the various coupling constants for TlF are given in Table II. The energy levels obtained by diagonalizing this Hamiltonian in a magnetic field of 15 G and a parallel electric field of 40 V/cm are shown in Fig. 3. This diagram is needed in our discussion of the state selector regions in Sec. III C.

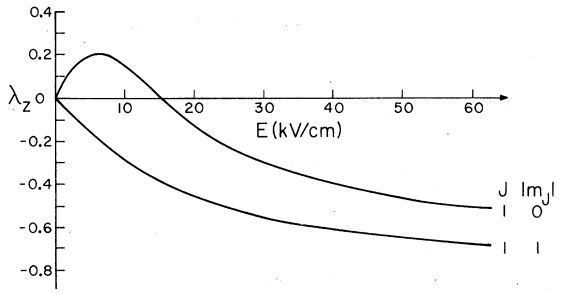

FIG. 2. Polarization of TlF in the $J=1$ states by an external electric field.

III. APPARATUS

A. General outline

Figure 4 shows the basic features of the beam apparatus, namely the source, detector, A, B, and C regions. TlF vapor in the hot oven effuses out of an array of slits to form a molecular beam. The beam passes through the A region which to a reasonable approximation only transmits molecules in a chosen magnetic sublevel of the hyperfine structure, namely (J,m_J,m_1,m_2) $=(1,-1,+\frac{1}{2},-\frac{1}{2})$. These selected molecules pass next through the C region where separated oscillating magnetic fields[16] induce a Tl nuclear-spin transition to state $(1,-1,-\frac{1}{2},-\frac{1}{2})$. A second state selector, the B region, transmits only the unresonated molecules which are then counted using a hotwire surface ionization detector and a parti-

TABLE I. Terms in the effective Hamiltonian for matrix elements diagonal in J (Ref. 22).

Rotational energy $= B\vec{\mathbf{J}}^2$
Stark shift $= d\hat{\lambda}\cdot\vec{\mathbf{E}}$
Zeeman shift $=\frac{-\mu_J}{J}(\vec{\mathbf{J}}\cdot\vec{\mathbf{B}})-\frac{\mu_1}{I_1}(\vec{\mathbf{I}}_1\cdot\vec{\mathbf{B}})-\frac{\mu_2}{I_2}(\vec{\mathbf{I}}_2\cdot\vec{\mathbf{B}})$
Spin-rotation interaction $= C_1(\vec{\mathbf{I}}_1\cdot\vec{\mathbf{J}})+C_2(\vec{\mathbf{I}}_2\cdot\vec{\mathbf{J}})$
Spin-spin tensor interaction $= C_3\left(\frac{3(\vec{\mathbf{I}}_1\cdot\vec{\mathbf{J}})(\vec{\mathbf{I}}_2\cdot\vec{\mathbf{J}})+3(\vec{\mathbf{I}}_2\cdot\vec{\mathbf{J}})(\vec{\mathbf{I}}_1\cdot\vec{\mathbf{J}})-2(\vec{\mathbf{I}}_1\cdot\vec{\mathbf{I}}_2)\vec{\mathbf{J}}^2}{\frac{1}{6}(2J+3)(2J-1)}\right)$
Spin-spin scalar interaction $= C_4(\vec{\mathbf{I}}_1\cdot\vec{\mathbf{I}}_2)$

TABLE II. Interaction constants for TlF in the $^1\Sigma$, $v=0$ states (Ref. 22).

$d = 4.228\,2(8)$ D
$\mu_j = \pm(25 \pm 11) \times 10^{-6}$ Bohr magnetons
$\mu_1 = 1.627\,34(42)$ nuclear magnetons [a]
$\mu_2 = 2.628\,50(5)$ nuclear magnetons [a]
$C_1/h = 126.03(12)$ kHz
$C_2/h = 17.89(15)$ kHz
$C_3/h = 0.70(3)$ kHz
$C_4/h = -13.30(72)$ kHz

[a] Taken from Ref. 18, Table VI. 1.

cle multiplier. Thus the beam intensity I at the detector is a measure of the nuclear transition probability in the C region.

The greatest sensitivity to a shift of the resonance is obtained by setting our oscillator frequency f on the steepest part of the resonance curve where $\partial I/\partial f$ is a maximum. Any small shift P of the resonant frequency then causes a maximum change in the detected beam intensity given by

$$\Delta I = -\left(\frac{\partial I}{\partial f}\right)_{\max} P . \tag{3}$$

The external fields E and B are independently reversed in complicated switching patterns[17] generated by an on-line computer. The computer analyzes the detected intensity I in such a way as to isolate ΔI, the intensity change which reverses with both E and B reversal, and which therefore indicates a violation of P and T. Equation (3) is then used to convert to a shift Δf of the resonant frequency.

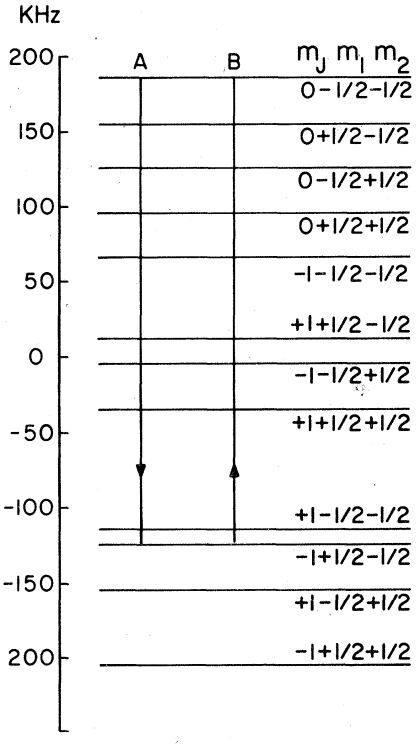

FIG. 3. Hyperfine structure of the $J=1$ states of TlF in the presence of parallel external magnetic and electric fields, $B=15$ G and $E=40$ V/cm.

A similar experiment has been done by Harrison *et al.*[18] Our hope in the present experiment was that by scaling up the beam apparatus, a substantial improvement in sensitivity could be obtained. In particular the separated oscillating fields, which drive the nuclear resonance, are 10 m apart in our apparatus resulting in a linewidth of only 20 Hz. Unfortunately, the sensitivity achieved by narrowing the resonance was offset by an unexpectedly large reduction in the resonance signal together with a high background rate. In spite of this we were able to obtain a final result which is equal in accuracy to that of Harrison.

B. Source and detector

The source is housed in a stainless steel chamber which is pumped to about 7×10^{-7} Torr by a 6 in. diffusion pump. The TlF is heated in a copper oven, stabilized within about 1°C at a temperature of about 340°C. The corresponding vapor pressures in the source are approximately 1.5×10^{-2} Torr for the monomer TlF and 5.7×10^{-2} Torr for the dimer $(TlF)_2$. A beam is formed by effusion of the vapor through an array of channels each 0.2 mm wide, 5 mm high, and 0.25 mm long. The array is 13 channels wide and 15 high with overall dimensions 5×80 mm. These channels were made from copper foil using photofabrication techniques.

Because our surface ionization detector dissociates the dimers we have no direct means of distinguishing one dimer from two monomers. However, if we make the reasonable assumption that the intensity is roughly proportional to $p/\sqrt{M}$, where p is the vapor pressure and M is the mass, the measured flux from our source is found to be

$$I_{\text{mono}} \simeq 3\times10^{16}\ (\text{TlF/sec})/\text{sr}, \tag{4a}$$

$$I_{\text{di}} \simeq 8\times10^{16}\ [(\text{TlF})_2/\text{sec}]/\text{sr}. \tag{4b}$$

In order to estimate what fraction of the beam is in a single $(J=1, m_J, m_1, m_2)$ sublevel it is reasonable to assume that the population of rotational states is given approximately by a Maxwell-Boltzman distribution at the temperature of the source. With this assumption one finds that only 10^{-4} of the monomer beam is able to take part in the resonance.

The surface ionization detector consists of a tungsten filament 7 mm wide and 80 mm high,

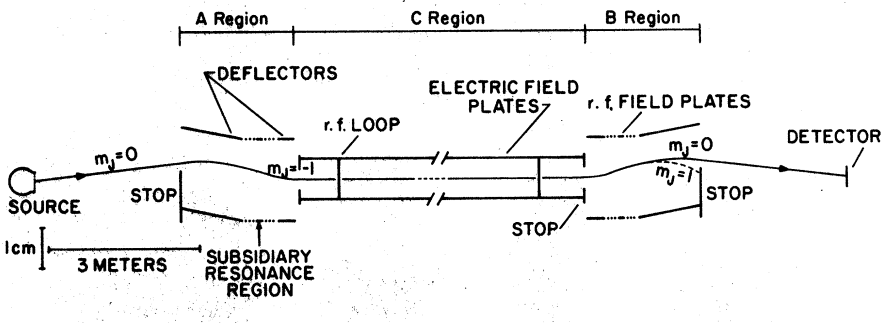

FIG. 4. Schematic diagram of the apparatus and beam trajectory.

heated to about 840°C. Tl^+ ions formed on the filament are focused electrostatically and then accelerated into a 60° magnetic sector mass spectrometer which discriminates against the background ions. The Tl^+ current is detected using an EMI 9603/2A particle multiplier. The pressure in the detector chamber is maintained at about 7×10^{-8} Torr.

In order to obtain adequate detection efficiency it is necessary to increase the work function of the filament by heating it to about 1100°C for a few minutes in an oxygen atmosphere. After this treatment the filament remains active for one or two days. The normal overall detection efficiency, defined as the number of detected Tl^+ ions divided by the number of Tl atoms incident on the filament, was measured to 20%–25% by the use of a small subsidiary oven in the detector region.

C. A and B regions

The purpose of the A region is to ensure that only those molecules in the state $(J, m_J, m_1, m_2) = (1, -1, +\frac{1}{2}, -\frac{1}{2})$ arrive at the C region. Basically the method used to discriminate between states is deflection in an inhomogeneous electric field. The deflecting force is

$$F_z = -d\langle\lambda_z\rangle \frac{\partial E_z}{\partial z}, \tag{5}$$

where d is the permanent electric dipole moment given in Table II and λ_z is the polarization given in Fig. 2. A simple deflector however is not adequate to distinguish between the various hyperfine sublevels, and therefore we use the more complicated arrangement shown in Fig. 4. Provided the hyperfine structure is resolved in the subsidiary resonance region this arrangement can use any $\Delta m_J=\pm1$ transition to select a single hyperfine substate.

In each of our subsidiary resonance regions there is a static magnetic field of 15 G and a parallel static electric field of 40 V/cm. Thus the energy levels in these regions are those shown in Fig. 3. The transitions which we have chosen to use are those indicated in Fig. 3; $(J, m_J, m_1, m_2) = (1, 0, -\frac{1}{2}, -\frac{1}{2}) \rightarrow (1, -1, \frac{1}{2}, -\frac{1}{2})$ in the A region and its inverse in the B region. In each case the transition is driven by a parallel oscillating electric field (0.8 V/cm rms), tuned to the energy level difference (310 kHz). We point out that it is the presence of the dc electric field which allows this nominally parity conserving transition to be induced by an oscillating electric field.

The deflectors are made of aluminum to the standard "two-wire" design.[16] Working potentials are ±27 kV resulting in an average field gradient of 2.6 kV/cm^2, constant within ±10% over the height of the beam and the width of the gap. Note that the field gradients in the long and short deflectors are oppositely directed although the fields are parallel.

The electric field is varied smoothly between 27 kV/cm and 40 V/cm on each side of each subsidiary resonance region by means of three short pairs of field plates. The central pair of plates provides the required rf field. A Watson electromagnet,[19] not shown in Fig. 4, supplies the 15 G magnetic field used to resolve the magnetic hyperfine structure. The pressure in the A and B regions is about 2×10^{-7} Torr.

D. C region

This region is one of large uniform electric field (26 kV/cm) and small magnetic field, in which the nuclear transition $m_1 = +\frac{1}{2} \rightarrow -\frac{1}{2}$ is induced by separated oscillating magnetic fields parallel to the beam axis. The electric field is provided by 10 cm high aluminum plates held 1 cm apart by Teflon insulators. Stops at each end allow a 5 mm wide beam to pass down to the center of the gap. The whole region is enclosed in a double Mumetal shield which keeps the magnetic field below 5×10^{-5} G after careful de-Gaussing (see Sec. 5).

The rf magnetic fields are provided by two 15-cm diameter coils of 50 turns each. When the two coils are fed coherently, the resulting resonance line shape is modulated by an interference pattern,[16] which effectively narrows the line and correspondingly increases sensitivity to small shifts of the resonance frequency. A large 8.8 m sep-

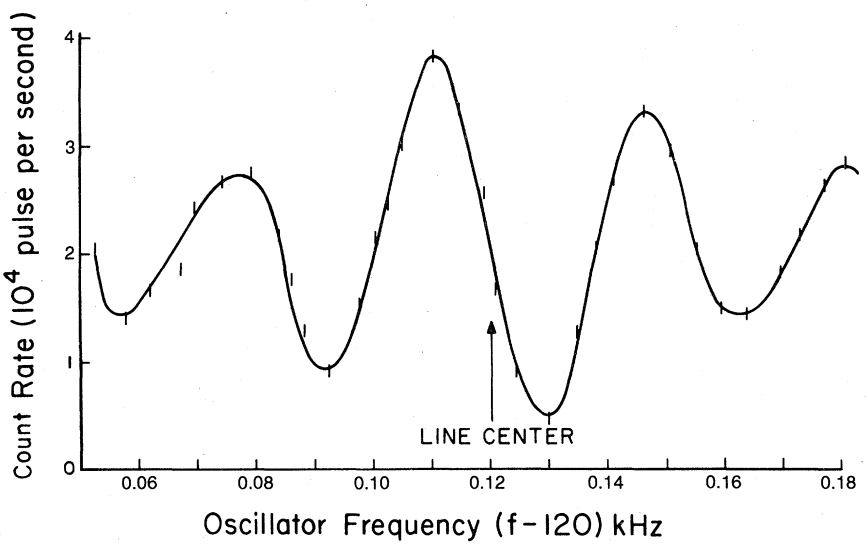

FIG. 5. Main resonance line shape with a phase shift between rf magnetic fields of approximately 90°.

aration between our rf loops leads to a linewidth of only about 20 Hz. Figure 5 shows the nuclear resonance line shape measured with 75 mA rms in each coil and with a phase angle of about 90° between the rf fields.

E. Sensitivity

The detected beam intensity is given by

$$I=N(1-c)+B, \tag{6}$$

where N is the number of beam molecules detected per second with no C resonance, c is the C resonance probability and B is the background rate. Suppose we count for a time $T/2$ and then, after reversing the electric field, for a further time $T/2$. The accumulated difference signal due to the shift P of Eq. (2) is

$$\Delta I\frac{T}{2}=N\frac{T}{2}\frac{\partial c}{\partial f}P. \tag{7}$$

Assuming Poisson statistics the total noise in this same period is approximately $(BT)^{1/2}$ since in our case B is the major part of I. The corresponding noise in the measured frequency shift is

$$\sigma=2B^{1/2}T^{-1/2}/N\left(\frac{\partial c}{\partial f}\right). \tag{8}$$

In a typical run the measured resonance slope $N(\partial c/\partial f)$ is approximately 1.5×10^3 (counts/sec)/Hz and the background B is 6×10^6 counts/sec. These figures give $\sigma\approx3T^{-1/2}$ Hz.

IV. EXPERIMENTAL METHOD

Our aim is to look for a resonance frequency shift arising from a P and T violating interaction. Such an effect is likely to be small and in measuring it one must expect to deal both with noise and with various systematic shifts whose origins are not P and T violating. We use a sophisticated control and analysis system based on a PDP8 computer to help eliminate systematic shifts and to accumulate data automatically for long periods of time. This system has been described in some detail by Harrison *et al.*[17]

The fundamental method of this experiment is to set the oscillator frequency to the steepest point on the line shape and look for changes in signal intensity. If any interaction of the form $\hat{\sigma}\cdot\hat{\lambda}$ is present, a reversal of the electric field should cause an intensity change. However, a dependence of the total beam intensity on the direction of the electric field will also produce a change in signal intensity. Here we are considering systematic effects, caused by the equipment which reverses the electric field, which of course would not occur in an ideal experiment. Our method of distinguishing these effects is to measure the shift again with the sign of the resonance slope reversed. In this case the beam intensity effect will be unchanged while the shift of interest has opposite sign. The sign of the resonance slope is most easily reversed by changing the relative phase of the two rf fields[20] from +90° to −90°.

Another systematic error results from inexact reversal of the electric field due, for example, to contact potentials which do not reverse. This leads to a shift because the nuclear resonance frequency depends, albeit weakly, on the electric field strength. In order to deal with this effect we reverse the magnetic fields in the subsidiary resonance regions, and hence we reverse the direction of the axis of quantization in the C region. This leaves the systematic effect in question unchanged,

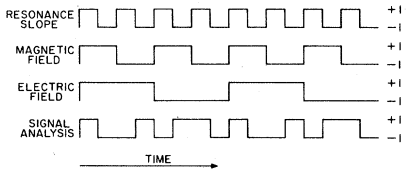

FIG. 6. Example of simple control and analysis waveforms.

but changes the sign of a genuine $\hat{\sigma} \cdot \hat{\lambda}$ shift.

Figure 6 shows a set of switching waveforms, the first three of which could be used in our automatic system to reverse the resonance slope, the magnetic field direction and the electric field direction. If all three modulations are simultaneously applied it follows from the discussion above that the sign of the shift at any moment due to a $\hat{\sigma} \cdot \hat{\lambda}$ interaction is given by the product of the signs of the three switching waveforms. This product waveform is the fourth one in Fig. 6. When the detected signal intensity is multiplied by the product waveform we obtain a signal whose dc component is the intensity change of interest.

We need to know the slope of the resonance curve since the measured intensity change has to be converted to a frequency shift. For this purpose an additional switching waveform is used to modulate the frequency of the rf oscillator by a known small amount, Δf. An analysis waveform obtained from the product of the calibration and resonance slope switching waveforms is used to detect the intensity change corresponding to this shift.

The signal is gated during and immediately after the switching of any experimental parameter to prevent the detection of transients.

An important feature of these waveforms is their orthogonality as discussed in detail by Harrison *et al.*[17] This is the basic feature which leads to the cancellation of the systematic effects. It also means that the primary experiment and the calibration of the resonance slope can proceed simultaneously without interfering with each other.

Two other analysis waveforms are used. The first is identical to the resonance slope switching waveform and therefore yields a signal equal to the intensity change caused by reversing the resonance slope. This signal, which is zero at the center of the resonance,[20] is used in a feedback loop to keep the oscillator locked onto the resonance. We are careful, of course, to lock to the average resonance frequency and not to follow the shift we are trying to measure. The second analysis waveform is quite unrelated to any of the switching waveforms and provides an independent measure of the noise.

It is desirable in practice not to use the simple square waves shown in Fig. 6 for switching but rather to use waveforms which are products of several square waves like the analysis waveform in Fig. 6. In effect this amounts to using a square wave which suffers periodic phase reversals and it serves to eliminate certain types of systematic error. Suppose for example that when the electric field is switched from state +1 to −1 the beam intensity momentarily drops. With the switching waveforms shown in Fig. 6 this effect always occurs in a +1 phase of both the resonance slope and magnetic field and, if it is not entirely gated out, will produce a systematic error in our result. Clearly such an error is eliminated by periodic phase reversals of the waveforms involved.

Harrison *et al.*[17] have shown that the undesirable effects of slow drifts in the beam and background intensities are also suppressed by the use of more complicated switching waveforms.

The noise in an ideal system of this type would be just the statistical noise of the detected signal but in reality additional noise arises from nonstatistical fluctuations. The noise spectrum of the detected intensity is found to be essentially flat above a few Hz with a sharp rise at low frequency. For this reason it is desirable to reverse at least one of the controlled parameters as frequently as possible. The reversal frequency of the resonance slope is limited only by the gated time delay between the second rf loop, where the phase is switched, and the detector. We use a 44.6 msec gating period and a minimum period of 134 msec in the resonance slope control waveform. With these settings the data collection time is $\frac{2}{3}$ of the real time. In practice this modulation is not as rapid as one would like and the actual noise level is about twice the statistical limit.

V. RESULTS

Table III shows the results of nine runs which took place on four separate days. In the runs labeled A the electric field was fixed parallel to the direction of the magnetic field in its +1 phase. In the B runs the electric field was fixed in the reverse direction. Automatic electric field reversal was used in run 5. We define shift P which changes sign when $\vec{E}$ or $\vec{B}$ or the resonance slope is switched; this of course is the shift of interest. We also define shift Q which changes sign with the switching of the resonance slope or $\vec{B}$ but not when $\vec{E}$ is reversed; this type of shift is caused, for example, by a stray static magnetic field in the C region.

Runs 1 and 2 revealed the presence of a shift Q of order 400 mHz, more than twice the noise level. The shift is consistent with a stray field of roughly 10^{-4} G in the C region. After run $2B$ we carefully

TABLE III. Raw results. Noise is given at the 1σ level.

Run $N^{\underline{0}}$	Type	Measured shift (mHz)	Noise check (mHz)
1A	$Q+P$	+193 ± 185	189
1B	$Q-P$	+523 ± 332	296
2A	$Q+P$	+591 ± 212	257
2B	$Q-P$	+335 ± 234	344
3A	$Q+P$	+293 ± 309	244
3B	$Q-P$	+61 ± 236	231
4A	$Q+P$	−23 ± 295	240
4B	$Q-P$	+235 ± 295	375
5	P	−103 ± 206	235

demagnetized the Mumetal shields which surround the C region and in the subsequent runs 3 and 4 the shift Q was not distinguishable from the noise. These results are presented in Table IV.

Each result shown in Table III is the result of a 40-min run during which the data were printed out every 80 sec. The error quoted on the measured shift is the observed standard deviation of the signal accumulated in the shift channel. As a method checking the noise level we also accumulate a signal in a noise channel which uses an analysis waveform of similar structure to that used in the shift channel but orthogonal to all induced shifts. Analysis of the noise channel data indicates that the noise is random and that the standard deviation of the shift channel provides a good estimate of the accuracy of our result.

Our final results for shift P are given in Table IV. The mean shift $\langle P\rangle_{av}$ is

$$\langle P\rangle_{av} = (21 \pm 84)\ \text{mHz}, \tag{9}$$

a suitably weighted average of the five results in Table IV.

The total amount of time spent on data accumulation in this experiment has not been as great as one might hope because of the experimental difficulty of optimizing a resonance which is so much smaller than the background. The considerable precision of our final result has not been obtained by measuring intensity changes minute compared with the height of the resonance, but rather reflects the narrowness of the resonance. That is also presumably the reason that systematic errors have not posed any real difficulty at this level.

TABLE IV. Final results.[a]

Run $N^{\underline{0}}$	Shift Q	Shift P	Error
1	+358	−165	190
2	+463	+128	158
3	+177	+116	213
4	+106	−129	189
5	-	−103	206

[a] Average shift $\langle P\rangle_{av} = (21 \pm 84)$ mHz.

VI. INTERPRETATION OF RESULTS

Using Eq. (2), we write the relation

$$hP = -4d\lambda_z \tag{10}$$

in which λ_z is the polarization given in Fig. 2. The electric field used in this experiment is 26 kV/cm, where $\lambda_z = -0.50$. It follows from Eqs. (9) and (10) that

$$d/h = (11 \pm 42)\ \text{mHz}. \tag{11}$$

In the preceding paper we calculate the value of d assuming that the proton has a permanent electric dipole moment d_p parallel to its spin. Two physically different contributions to d are distinguished, namely, the volume effect

$$d^V/h = 5.1\times 10^{18} d_p\ \text{Hz} \tag{12}$$

and the magnetic effect

$$d^M/h = 8.5\times 10^{17} d_p\ \text{Hz}, \tag{13}$$

where d_p is in e cm. Assuming $d = d^V + d^M$ we find

$$d_p = (1.8 \pm 7)\times 10^{-21}\, e\ \text{cm}. \tag{14}$$

Since the size of the volume effect depends on the rather uncertain nuclear integral, R (see Sec. III B of the preceding paper), one might wish to take a conservative view and calculate a value for d_p based only on the magnetic effect which is completely insensitive to the details of the nuclear structure. In that case Eqs. (11) and (13) give

$$d_p = (1.3 \pm 5)\times 10^{-20}\, e\ \text{cm}. \tag{15}$$

When the result in Eq. (14) is combined with Harrison's result,[18] $d_p = (-7 \pm 9)\times 10^{-21} e$ cm, we obtain the best estimate of the proton electric dipole moment:

$$d_p = (-1.4 \pm 6) \times 10^{-21}\, e \text{ cm}. \quad (16)$$

This compares to the limit $|d_p| < 5.5 \times 10^{-19}\, e$ cm determined by Khriplovich[21] from the limit on the electric dipole moment of the cesium atom.

An alternative interpretation of our result involves a weak P and T violating neutral current tensor interaction between electrons and protons

$$H_T = iC_T (G_F/\sqrt{2}) \bar{\Psi}_p \Gamma_T \Psi_p \bar{\Psi}_e \Gamma_T \Psi_e \delta(\vec{r}_{e,p}), \quad (17)$$

where Γ_T is the usual antisymmetric tensor combination of Dirac matrices. As we have discussed more fully elsewhere[1] this interaction in TlF may be written in the form of Eq. (2) with a coupling constant d^T given by

$$d^T/h = 1.4 \times 10^3 C_T \text{ Hz}. \quad (18)$$

This result taken together with Eq. (11) gives

$$C_T = (0.8 \pm 3) \times 10^{-5}. \quad (19)$$

Equations (16) and (19) represent the most accurate values to date for d_p and C_T.

ACKNOWLEDGMENTS

This work was supported by the Science Research Council at Oxford University and in part by the National Science Foundation at Yale University under Grant No. PHY75-02376 A01.

*Present address: Physics Dept., Yale Univ., New Haven, Conn. 06520.

[1]E. A. Hinds, C. E. Loving, and P. G. H. Sandars, Phys. Lett. B 62, 97 (1976).
[2]J. H. Christenson, J. W. Cronin, V. L. Fitch, and R. Turlay, Phys. Rev. Lett. 13, 138 (1964).
[3]R. C. Casella, Phys. Rev. Lett. 21, 1128 (1968); R. C. Casella, Phys. Rev. Lett. 22, 554 (1969).
[4]N. F. Ramsey, Phys. Rep. 43, 410 (1978), and references therein.
[5]L. I. Schiff, Phys. Rev. 132, 2194 (1963).
[6]P. G. H. Sandars, Phys. Rev. Lett. 19, 1396 (1967).
[7]M. A. Bouchiat and C. Bouchiat, J. Phys. (Paris) 35, 899 (1974).
[8]V. A. Alekseev, B. Ya. Zel'dovich, and I. I. Sobel'man, Sov. Phys. Usp. 19, 207 (1976).
[9]A. N. Moskalev, R. M. Ryndin, and I. B. Khvipolovich, Sov. Phys. Usp. 19, 220 (1976).
[10]L. M. Barkov, I. B. Khriplovich, and M. S. Zolotorev, Comments At. Mol. Phys. 8, 79 (1979).
[11]N. Fortson, Bull. Am. Phys. Soc. 24, 40 (1979).
[12]P. G. H. Sandars, in *Unification of Elementary Forces and Gauge Theories*, edited by D. Cline and F. Mills (Harwood Academic, London, 1977), p. 153.
[13]R. Conti, P. Bucksbaum, S. Chu, E. Commins, and L. Hunter, Phys. Rev. Lett. 42, 343 (1979).
[14]C. Y. Prescott *et al.*, Phys. Rev. Lett. B 77, 347 (1978).
[15]H. K. Hughes, Phys. Rev. 72, 614 (1947).
[16]N. F. Ramsey, *Molecular Beams* (Oxford University Press, London, 1963).
[17]G. E. Harrison, M. A. Player, and P. G. H. Sandars, J. Phys. E 4, 750 (1971).
[18]G. E. Harrison, P. G. H. Sandars, and S. J. Wright, Phys. Rev. Lett. 22, 1263 (1969).
[19]I. I. Richmond and D. W. Parker, in *Proceedings of the Second International Conference on Magnet Technology* (Oxford University Press, London, 1967).
[20]N. F. Ramsey and H. B. Silsbee, Phys. Rev. 84, 506 (1951).
[21]I. B. Khriplovich, Sov. Phys. JETP 44, 25 (1976).
[22]G. Gräff, W. Paul, and C. H. Schlier, Z. Phys. 153, 38 (1958).